ARTICLE OPEN

Check for updates

A facile strategy for fabrication of nanocomposite ultrafiltration membrane: oily wastewater treatment and photocatalytic self-cleaning

Umair Baig[1✉] and Abdul Waheed [1✉]

Understanding the importance of reclaiming water from a huge oily wastewater stream generated during the drilling of oil in the petroleum industry and mitigating membrane fouling, a polymeric-inorganic nanocomposite membrane was fabricated with self-cleaning properties. The photocatalytic TiO_2 nanoparticles were embedded in the polyvinylidene fluoride (PVDF) matrix during wet phase inversion. To enhance the separation potential and photocatalytic activity of TiO_2 nanoparticles, a conjugated polypyrrole (PPy) was grown on the membrane through oxidative polymerization leading to an active layer composed of $PPy@TiO_2$ nano-photocatalyst. The study of membrane wettability revealed the hydrophilic and underwater superoleophobic nature of the $PPy@TiO_2/PVDF$ membrane. The $PPy@TiO_2/PVDF$ membrane was applied for treating water-containing emulsified oily feed. Different types of feeds contaminated by different oils such as motor oil, diesel oil, and crude oil were studied. The separation efficiency of the $PPy@TiO_2/PVDF$ membrane stayed above 99% as the membrane allowed only water to permeate while oil was rejected. The permeate pure water flux was found to be dependent upon feed pressure and the nature of oil in the feed. While keeping the separation efficiency constant at 99%, the flux was decreased with increasing concentration of oil in the feed which is attributed to the fouling of the membrane. The fouled membrane was photo-catalytically cleaned by exposing the fouled $PPy@TiO_2/PVDF$ membrane to solar-simulated visible light as the surface features of the cleaned membrane completely resembled that of the pristine $PPy@TiO_2/PVDF$ membrane.

INTRODUCTION

Rapid industrial development has led to several challenges for human beings in the current era of urbanization followed by industrialization[1]. Oil spills and the generation of immense quantities of emulsified oily wastewater including produced water (oil in water; O/W emulsion) are some of these challenges[2]. Treating such wastewater streams will not only generate clean water but it will also minimize environmental pollution. Furthermore, the recovery of clean water from O/W emulsions will also lower the stress on dwindling freshwater resources[3]. Many approaches such as dissolved air floatation, chemical methods, bioremediation, gravity filtration through meshes, and the use of sponges and sorbents have been explored in literature for the separation of oil from oil/water emuslion[4].

In one such approach, superhydrophobic and superoleophilic materials have been designed which preferably allow oil to pass through while water is repelled by the material[5]. Although such materials have proved to be highly efficient for O/W separation, the excessive fouling of such materials due to the deposition of oil is a huge challenge that lowers the separation performance of such materials. In one such work, Zhan et al. synthesized a TiO_2-gelatine-based aerogel that was not only able to remove both cationic and anionic dyes but also to separate oil from both oil/water-free mixtures and O/W emulsion. However, the TiO_2-gelatine-based aerogel was also able to degrade the adsorbed pollutants leading to efficient regeneration of the aerogel[6].

Another highly important variant of surface wettability of materials is the superhydrophilicity/hydrophilicity and underwater superoleophobicity which allows the water to permeate through while oil is repelled back by the materials[7]. This mode of surface wettability is advantageous as the superhydrophilic/hydrophilic surface does not allow the oil to wet the surface and hence the evidence of oil fouling and deposition on the material surface are minimized to a larger extent. In one such instance, J. Jin et. al. developed a mesh membrane made up of cupric phosphate ($Cu_3(PO_4)_2$) having a superhydrophilic nature with a contact angle (CA) of zero. However, the cupric phosphate mesh membrane also possessed an underwater superoleophobic nature with an oil contact angle (OCA) of >158° which allowed the water to pass through the mesh while oil water rejected with a permeate containing 2 ppm oil in it[8]. In another work, Z. Zhang et. al. developed a superhydrophilic sponge with underwater super-oleophobic surface wettability. The sponge was developed through in-situ growth of TiO_2 nanocrystals followed by vapor deposition of polypyrrole (PPy) leading to multifunctional $MS@TiO_2@PPy$. The sponge was able to separate oil dispersed in O/W mixtures with a permeate flux reaching 9549 L m^{-2} h^{-1} (LMH)[4].

The incorporation of nanoparticles (NPs) such as TiO_2 in the membranes or meshes has added an advantage to photocatalysis[9]. Certain NPs such as TiO_2, $BiVO_3$, and Fe_2O_3 have been used as traditional photocatalysts that are usually excited by ultraviolet (UV) irradiation which is due to a wide band gap 3.2 eV (TiO_2)[10,11]. This lowers the application of such NPs in real-life applications as natural sunlight contains merely 3–5% UV when it reaches the Erath's surface. The incorporation of the photocatalysts in the porous matrix has been reported to be advantageous as there are

fewer chances of agglomerated NPs, high light absorption, and lower possibility of catalyst leaching during filtration experiments. Furthermore, the inclusion of conjugated polymers such as PPy can also augment the photocatalytic ability of TiO$_2$@PPy leading to the degradation of pollutants[11]. Previously, such NPs have been incorporated in the sponges which have lower chances of application in the real world as unlike the pressure-driven separation, the sponges are applied under gravity[12]. The gravity separation can work for small-volume mixtures of oil and water while its application using larger volumes of feeds is not feasible. The gravitational force with large volumes of feed can easily overcome the resistance offered by sponges and meshes which can over-turn the separation capability of such materials. Hence, the need of the day is to come up with a strategy where photocatalytic NPs are decorated stably in the membrane which can work under pressure and have ideal features of being superhydrophilic/hydrophilic, underwater superoleophobic, and photocatalytic in nature. We designed an approach to not only deposit TiO$_2$ nanoparticles in the membrane matrix but also make its composite with conjugated polymer polypyrrole (PPy) yielding PPy@TiO$_2$ onto the membrane. This approach not only led to a stable decoration of TiO$_2$ but its composite PPy@TiO$_2$ has also led to excellent self-cleaning properties for removing fouling due to oil deposition. Hence, the membrane decorated with PPy@TiO$_2$ can be efficiently regenerated and reused for treating oily wastewater streams.

Given the above discussion, we have developed a new polymeric-inorganic nanocomposite membrane by decorating the TiO$_2$ NPs in the matrix of polyvinylidene fluoride (PVDF) ultrafiltration membrane which was coated by PPy. The TiO$_2$ NPs were deposited in the PVDF matrix during phase inversion. The TiO$_2$-containing PVDF membrane was decorated and coated with PPy particles generated through in-situ oxidative polymerization of pyrrole monomer leading to the PPy@TiO$_2$/PVDF Membrane. The presence of PPy@TiO$_2$ in the PVDF membrane imparts not only hydrophilic features to the membrane but also photocatalytic self-cleaning properties along with excellent separation of O/W surfactant stabilized emulsion. Following a thorough characterization of the membrane, the PPy@TiO$_2$/PVDF/PET membrane was applied for O/W surfactant-stabilized emulsion separation. Different types of oil feeds including motor oil, diesel oil, and crude oil were used during filtration experiments. The effect of increasing oil concentration and feed pressure on the performance of the membranes was also studied. The performance of the membrane was compared with the two other membranes bare PVDF and TiO$_2$/PVDF membranes fabricated in this work.

RESULTS AND DISCUSSION

The polymeric organic/inorganic nanocomposite membrane was fabricated by incorporating TiO$_2$ in the PVDF matrix during phase inversion followed by oxidative growth of a polymeric active layer of PPy as shown in Fig. 1. The presence of TiO$_2$ nanoparticles in the PVDF matrix led to the strong interaction between the PPy layer and PVDF which is attributed to hydrogen bonding between N-H of pyrrole moiety and O-H group of TiO$_2$. Moreover, the C-F bond of PVDF also acts as an H-bond acceptor. The possible structure and H-bonding are shown in the following Fig. 2a.

One of the characteristic identifications of the structure of the materials is the presence of specific functional groups which are identified through FTIR. In the case of both support and the resultant membranes, the ATR-FTIR spectra were recorded as given in Fig. 2b. The presence of the TiO$_2$ was justified by a sharp and deep band at 480 cm^{-1} which is attributed to the bending mode of the Ti-O bond[13]. The peaks at around 760 cm^{-1} and 840 cm^{-1} represent α and β phases of PVDF in addition to peaks at 1220 cm^{-1} and 1400 cm^{-1} (Fig. 2b)[14]. All these peaks were also found in the case of the PPy@TiO$_2$/PVDF membrane. However, a

new peak appeared at around 1550 cm^{-1} which is attributed to the characteristics vibration band of the pyrrole ring[15].

Another highly useful information regarding the surface chemistry of the membranes is the hydrophilicity of the membranes. For the sake of understanding the hydrophilic nature of the membrane, both water and oil contact angles were measured in air and underwater media (Fig. 3). The water contact angle in air (WCA = $\theta_{W, A}$) of the three membranes was recorded. A decreasing trend in WCA = $\theta_{W, A}$ was recorded as follows PVDF > TiO$_2$/PVDF > PPy@TiO$_2$/PVDF membrane with values of 119.6°, 93.1°, and 52.7° respectively (Fig. 3a). This observation confirmed that the surface hydrophilicity of the membrane increases with the inclusion of TiO$_2$ and PPy. Hence, the current approach of fabricating a membrane changed the surface wettability of the PVDF membrane from hydrophobic to hydrophilic. Similarly, the oil contact angle in air (OCA = $\theta_{O, A}$) of all the membranes including PVDF, TiO$_2$/PVDF, and PPy@TiO$_2$/PVDF membrane revealed the superoleophilic nature of the membranes. The values of $\theta_{O, A}$ were found to be 0°. A very interesting finding was the measurement of underwater oil contact angles ($\theta_{O, W}$) of all the membranes which were measured to be 0°, 132.4°, and 160° for PVDF, TiO$_2$/PVDF, and PPy@TiO$_2$/PVDF membrane. This measurement confirmed that the PVDF membrane is superoleophilic even underwater and hence cannot serve the purpose of separating oil from water in the case of surfactant stabilized O/W emulsion. However, after including the TiO$_2$ nanoparticles membrane demonstrated a certain level of oleophobicity ($\theta_{O, W}$ = 132.4°) underwater of TiO$_2$/PVDF membrane which increased further ($\theta_{O,W}$ = 160°) on depositing PPy confirming the underwater superoleophobic nature of the PPy@TiO$_2$/PVDF membrane. These observations of varying surface wettability behavior of the membrane can be attributed to the presence of several components in the membrane. The hydrophilic nature of the PPy@TiO$_2$/PVDF membrane can be attributed to the presence of numerous hydrophilic groups such as -OH and -NH of TiO$_2$ and PPy. Similarly, the superoleophilic nature of the PPy@TiO$_2$/PVDF membrane might be due to the highly porous polymeric layer allowing penetration of oil into the membrane in an air medium. The underwater superoleophobic behavior of the PPy@TiO$_2$/PVDF membrane can be justified by considering the hydrophilic nature of the membrane. Upon dipping the PPy@TiO$_2$/PVDF membrane in water, the hydrophilic nature of the membrane allowed rapid penetration of water into the membrane which in turn provides cushion to oil and hence blocks the entry of oil into the membrane[16]. Figure 3b shows the digital images captured during contact angle measurement experiments.

To further explore the surface features of the PPy@TiO$_2$/PVDF membrane, atomic force microscopy (AFM) was measured as shown in Fig. 4. The AFM images of bare PVDF (Fig. 4a, b), TiO$_2$/PVDF membrane (Fig. 4c, d), and PPy@TiO$_2$/PVDF (Fig. 4e, f) membrane were measured. It is obvious from both 2D (Fig. 4a) and 3D (Fig. 4b) images of the PVDF membrane that the average roughness (R_a) and root mean square roughness (R_q) was 56.1 nm and 82.1 nm respectively. However, after the inclusion of TiO$_2$ nanoparticles, both R_a and R_q of TiO$_2$/PVDF membrane were found to be increased to 66.2 nm and 84.9 nm, respectively. However, after the growth of PPy at TiO$_2$/PVDF membrane, the values of both R_a and R_q were increased further to values of 85.2 nm and 116 nm respectively. The increase in surface roughness is also obvious from 2D (Fig. 4e) and 3D (Fig. 4f) images of PPy@TiO$_2$/PVDF membrane. The increase in surface roughness of the PPy@TiO$_2$/PVDF membrane can be attributed to the polymeric growth of PPy on the bare TiO$_2$/PVDF membrane.

One of the salient features of membrane surface characterization is the surface morphology of the membrane. In a quest to know the surface morphologies of the membranes, SEM analysis of the three membranes PVDF, TiO$_2$/PVDF, and PPy@TiO$_2$/PVDF membranes was carried out as shown in the following Fig. 5. A highly porous PVDF membrane can be seen in the micrograph without the appearance of any nanoparticles in the membrane
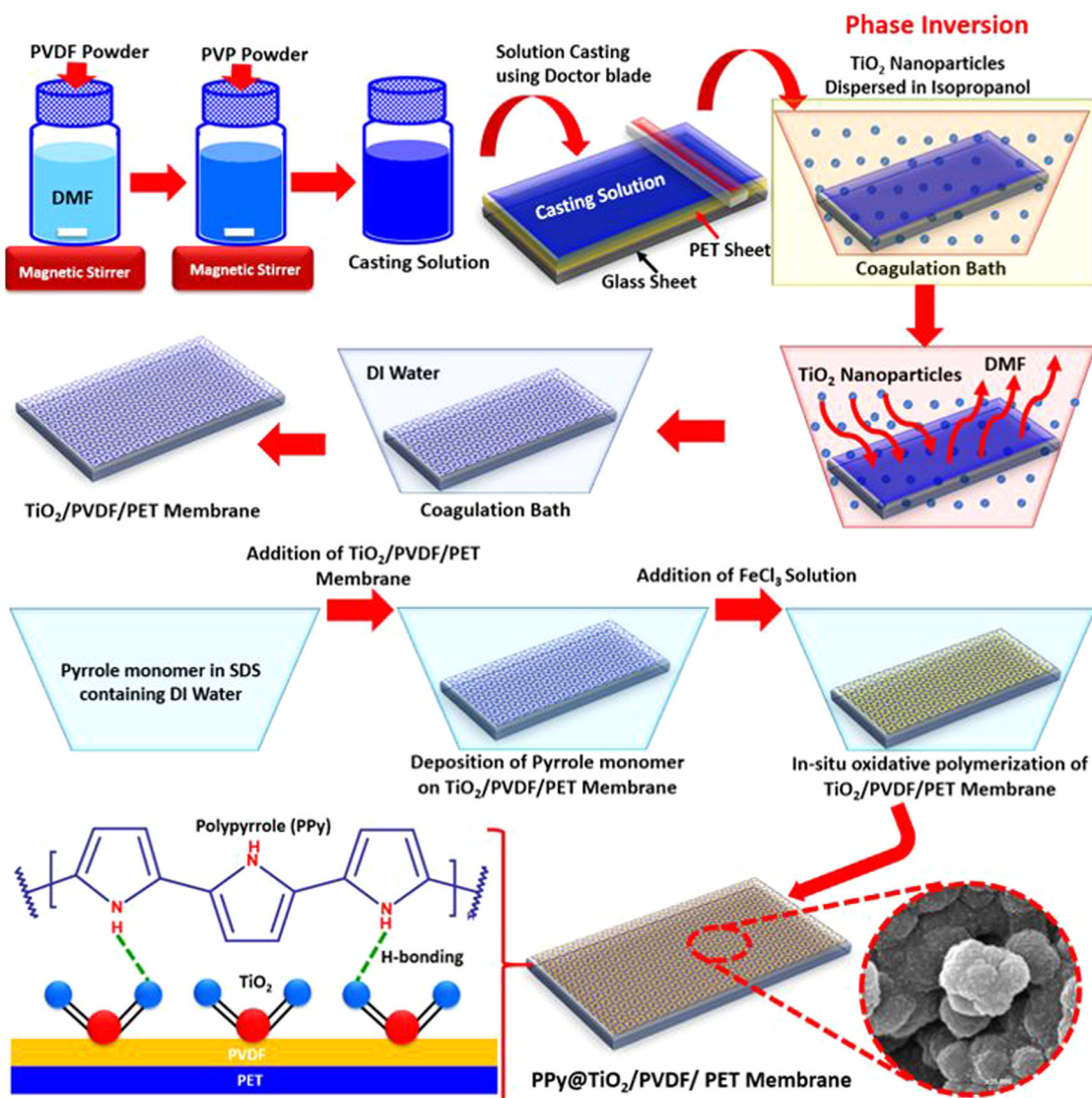
Fig. 1 Phases of membrane fabrication using phase inversion and oxidative polymerization. Image does not contain any third party material.

matrix (Fig. 5a–c). In the case of the TiO$_2$/PVDF membrane (Fig. 5d–f), the membrane matrix appeared to have TiO$_2$ nanoparticles decorated in each bit of the PVDF polymeric matrix. The high-resolution image of the TiO$_2$/PVDF membrane revealed a highly homogenous structure where TiO$_2$ nanoparticles appeared to have become an integral part of the PVDF matrix (Fig. 5f). A sponge-like pattern is visible both in PVDF (Fig. 5a) and TiO$_2$/PVDF (Fig. 5d) membranes which can be attributed to the wet phase inversion of PVDF dope solution. The presence of porous sponge-like channels provides a feasible passage for permeate to pass through the membrane. Furthermore, the channels of the TiO$_2$/PVDF membrane are decorated with TiO$_2$ nanoparticles which offer hydrophilicity to the membrane developing a strong attraction for water molecules. Upon oxidative polymerization of the pyrrole monomer, the spongy nature of the PPy@TiO$_2$/PVDF membrane is completely altered (Fig. 5g–i) which can be attributed to the development of a PPy layer on TiO$_2$/PVDF membrane. The globular nature of PPy is evident in high-resolution micrographs (Fig. 5i). The presence of globules in the PPy@TiO$_2$/PVDF membrane confirmed the success of oxidative polymerization of pyrrole monomer leading to the development of an efficient separation layer.

To dig further into the structure of the membrane, cross-sectional SEM micrographs of all the membranes are also presented in Fig. 6. As revealed by the surface SEM analysis, the top active layer shows almost similar pattern of morphology even in the cross-sections of the membranes. In the case of PVDF membrane (Fig. 6a–c), the sponginess of the membrane's active layer can be seen and as we move to higher magnifications (Fig. 6c), the polymeric network of PVDF is evident without any of the nanoparticles deposited in the polymeric framework. However, when we move to the TiO$_2$/PVDF membrane, not only are the polymeric chains organized into a more profound framework but the presence of TiO$_2$ nanoparticles is also evident (Fig. 6d–f). On moving onto the PPy@TiO$_2$/PVDF membrane, the PVDF polymeric framework is completely intermingled with the polymeric framework of PPy (Fig. 6g–i) in a way that it appears a completely merged composite active layer which is ideal for O/W emulsion separation. Moreover, the TiO$_2$ nanoparticles have also been completely wrapped by polymeric chains and hence the nanoparticles are uniformly distributed throughout the framework of the PPy@TiO$_2$/PVDF membrane. Hence, the current strategy of fabricating a membrane has resulted in a membrane with a uniform structure avoiding the formation of agglomerates and
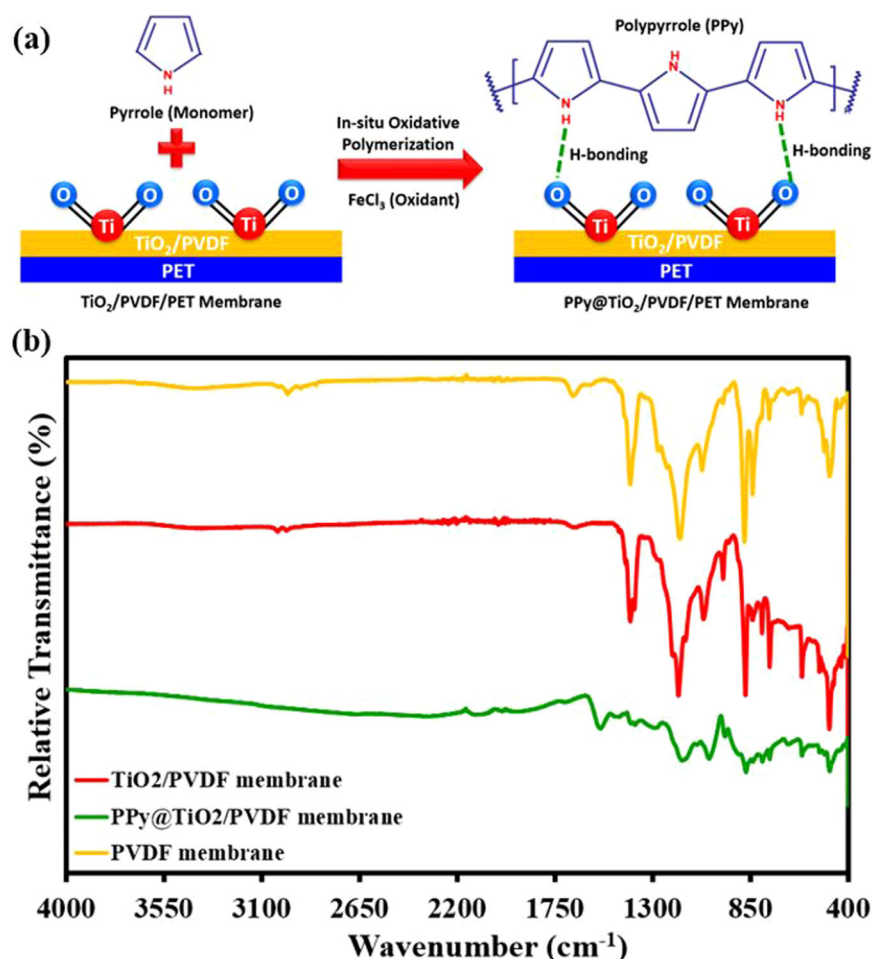
Fig. 2 Membrane structure and their FT-IR spectroscopic analysis. Proposed reaction and structure of PPy@TiO$_2$/PVDF membrane (**a**). ATR-FTIR of PVDF membrane, TiO$_2$/PVDF membrane and PPy@TiO$_2$/PVDF membrane (**b**).

defects in the membrane. This can also be attributed to the chemistry of the integral components involved in the fabrication of the PPy@TiO$_2$/PVDF membrane. There is a possibility for the formation of hydrogen bonding between the -OH groups of TiO$_2$, -NH groups of PPy, and -C-F bonds of PVDF. This hydrogen bonding leads to the formation of a stable, homogenous, and defect-free PPy@TiO$_2$/PVDF membrane. Beneath the active layer, the layer of the PET can also be seen in the case of all the membranes studied in this work which confirms the composite structure of the membranes. The purpose of the PET which is a non-woven fabric (evident from the fibers seen in cross-sectional SEM micrographs of all the membranes particularly in Fig. 6a, d, g) is to offer support during separation under crossflow filtration conditions.

EDX analysis of PVDF, TiO$_2$/PVDF, and PPy@TiO$_2$/PVDF membranes revealed the surface elemental composition of the membranes as shown in Fig. 7. EDX analysis of the PVDF membrane showed the presence of Carbon (N) and Fluorine (F) only (Fig. 7a, b) which is quite obvious because PVDF has only -C-C-F bonds in the polymer backbone that could be detected by EDX analysis. TiO$_2$/PVDF membrane confirmed the presence of all of the constituent elements including Carbon (C), Oxygen (O), Fluoride (F), and Titanium (Ti) as shown in Fig. 7c, d. Similarly, the EDX analysis of the PPy@TiO$_2$/PVDF membrane (Fig. 7e, f) indicated the presence of all the previously mentioned elements with Nitrogen (N) being an additional element which is attributed to the presence of PPy on the PPy@TiO$_2$/PVDF membrane. Furthermore, there was also an increment in the concentration

of O (12%) in the case of PPy@TiO$_2$/PVDF membrane compared to TiO$_2$/PVDF membrane with O reaching 8.3% (Supplementary Table 1). This can be attributed to the rearrangement of the polymeric framework of the PPy@TiO$_2$/PVDF membrane where PPy having more chances of hydrogen bonding with TiO$_2$ has attracted the TiO$_2$ nanoparticles to the surface penetrating growing PPy chains and hence the more O is detected in the PPy@TiO$_2$/PVDF membrane. This observation also supports the fact that there is considerable interaction between the components of the membrane involved in the fabrication of the PPy@TiO$_2$/PVDF membrane.

The elements detected by EDX analysis were found to be equally distributed throughout the membrane surface area as confirmed by elemental mapping of PVDF (Fig. 8a–c), TiO$_2$/PVDF (Fig. 8d–h), and PPy@TiO$_2$/PVDF (Fig. 8i–n). The elemental mapping also confirmed the presence of an additional element N (Fig. 8n) which is due to the growth of the PPy active layer in the case of the PPy@TiO$_2$/PVDF membrane.

Evaluation of Oil/water emulsion separation performance
Following thorough characterization and establishing the structure of all the fabricated membranes PVDF, TiO$_2$/PVDF, and PPy@TiO$_2$/PVDF membrane, the oil/water emulsion separation potential of the membranes was explored. The permeate flux of all the membranes increased with increasing transmembrane pressure. The permeate flux of bare PVDF membrane was found to be the highest among all the membranes reaching 28000 L.m^{-2}.h^{-1} (LMH) at 4 bar (Fig. 9a) which might be due to the absence of any

surface coating or active layer in the case of bare PVDF membrane. A slight decrease in permeate flux was observed upon the inclusion of TiO$_2$ nanoparticles. The PVDF and TiO$_2$/PVDF membranes were microporous due to the lack of an active layer. However, upon the growth of the PPy polymeric framework, the resultant PPy@TiO$_2$/PVDF membrane demonstrated an

ultrafiltration characteristic as the permeate flux decreased considerably. The PPy@TiO$_2$/PVDF membrane showed a permeate flux of 25 LMH to 280 LMH (Fig. 9b) at a transmembrane pressure of 1 bar to 4 bar, respectively.

Upon using a surfactant stabilized O/W emulsion as a feed at 2 bar, the permeate flux decreased compared to using DI water as feed. This shows that the oil developed an attraction with membrane surfaces and gets deposited leading to a reduction in permeate flux. The decrease in permeate flux was found to be almost similar in the case of all the membranes. The permeate flux of PVDF membrane was found to be 17000 LMH, 12000 LMH for TiO$_2$/PVDF and 28 LMH for PPy@TiO$_2$/PVDF membrane (Fig. 10a). However, in the case of O/W emulsion separation, PPy@TiO$_2$/PVDF membrane showed the highest separation efficiency reaching >99% compared 40% for TiO$_2$/PVDF membrane and a merely 8% separation efficiency for PVDF membrane (Fig. 10b). More clarity of the separation efficiencies of the membranes can be realized through the light microscopic images and digital photographs of feeds and emulsions. Figure 10c, d shows the dispersed oil droplets in water confirming the successful formation of O/W emulsion. In the case of permeates obtained from PVDF (Fig. 10e, f) and TiO$_2$/PVDF (Fig. 10g, h) membranes, the light microscopic images and digital photographs did not show any appreciable decrease in droplets and cloudiness. However, in the case of the PPy@TiO$_2$/PVDF membrane, there was a marked decrease in the oil droplets in the emulsion, and completely clear of any cloudiness yielding clean water (Fig. 10i, j).

To further investigate the potential of PPy@TiO$_2$/PVDF membrane for O/W emulsion separation, different types of oils were used as feed. Different oil feeds were prepared by dissolving an appropriate amount (200 ppm) of oil in water. It was found that flux decreased with the changing chemistry and matrix of the feed oil. Crude oil (CO) has a highly complex matrix and hence offers more chances of fouling. The other oils such as motor oil (MO) and diesel oil (DO) are just fractions of crude oil and hence the chances of developing the fouling layer over the membrane surface are lesser compared to CO which leads to an increase in permeate flux. Hence, MO showed the highest permeate flux of 29 LMH followed by DO and CO with permeate fluxes of 25 LMH and 17 LMH at 2 bar respectively (Fig. 11a). However, the separation efficiency of the PPy@TiO$_2$/PVDF membrane remained considerably high. In the case of all the tested feeds containing MO, DO,
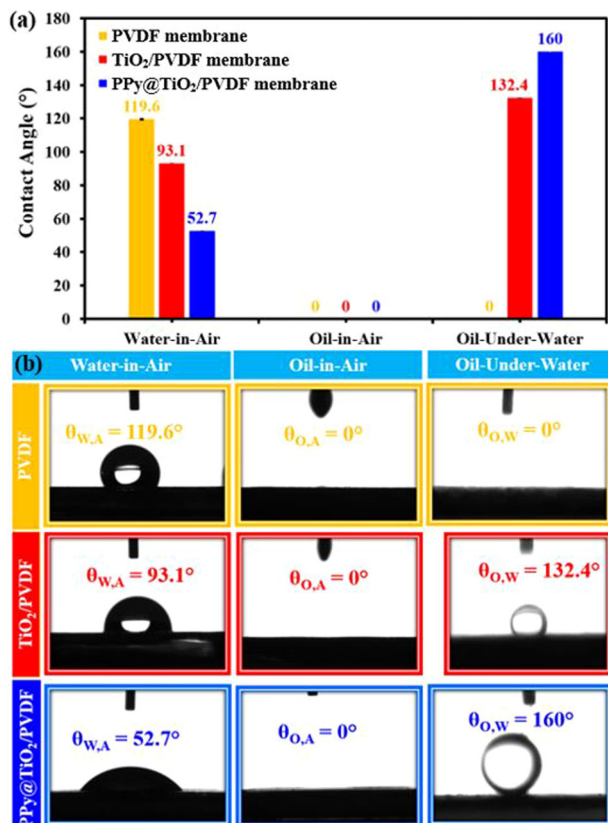


Fig. 3 Surface wettability analysis of the membranes. In air-water contact angle (WCA) and oil contact angle both in air and underwater of PVDF membrane, TiO$_2$/PVDF membrane, and PPy@TiO$_2$/PVDF membranes.
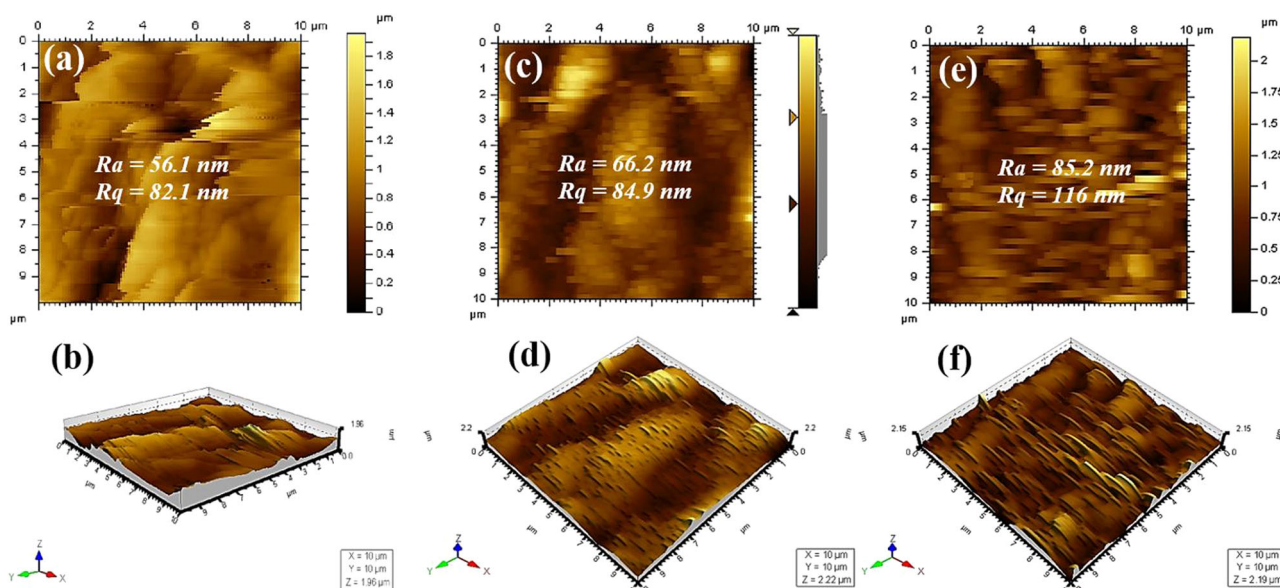
Fig. 4 AFM surface topological and roughness analysis of the membranes. AFM images of 2D (a) & 3D (b) of bare PVDF membrane, 2D (c) & 3D (d) of TiO$_2$/PVDF membrane, and 2D (e) & 3D (f) images of PPy@TiO$_2$/PVDF membrane.
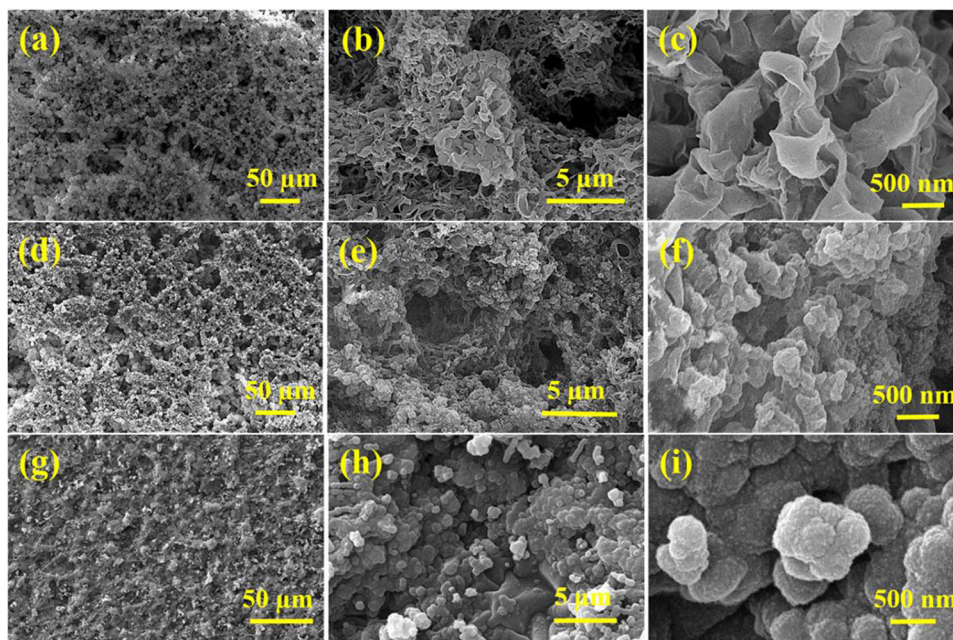
Fig. 5 Morphological analysis of the membranes. SEM micrographs of (**a**–**c**) PVDF membrane, (**d**–**f**) TiO$_2$/PVDF membrane, and (**g**–**i**) PPy@TiO$_2$/PVDF membrane.
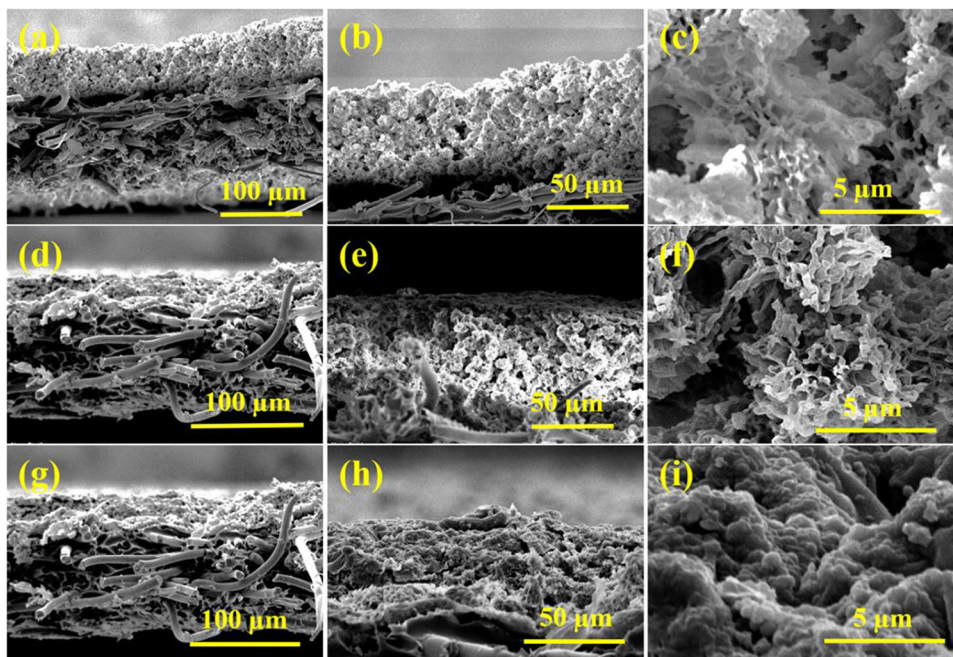

Fig. 6 SEM cross-sectional analysis of the membranes. Cross-section SEM images of (**a**–**c**) PVDF membrane, (**d**–**f**) TiO$_2$/PVDF membrane, and (**g**–**i**) PPy@TiO$_2$/PVDF membrane.

and CO, the rejection was found to be >99% (Fig. 11a). This higher separation efficiency of PPy@TiO$_2$/PVDF membrane can be attributed to the oxidative polymerization of Py yielding a PPy active layer as confirmed by AFM (Fig. 4) and SEM (Fig. 5) images. Moreover, the underwater superoleophobicity of the PPy@TiO$_2$/PVDF membrane led to the rejection of oil while allowing the water to permeate through the membrane.

Another important aspect of O/W emulsion separation experiments is the varying concentration of oil in the feed. We also studied the impact of increasing DO concentration (50 ppm, 100 ppm, and 200 ppm) of diesel oil in the O/W emulsion. It was found that with an increasing oil concentration in the feed, the flux of the permeate was gradually decreased which can be attributed to the building of a fouling layer on the PPy@TiO$_2$/PVDF membrane (Fig. 11b). However, the separation efficiency of the PPy@TiO$_2$/PVDF membrane remained nearly constant for all the tested feed types (11b). These findings suggest that the PPy active layer was able to reject even higher concentrations of oils in the feeds.
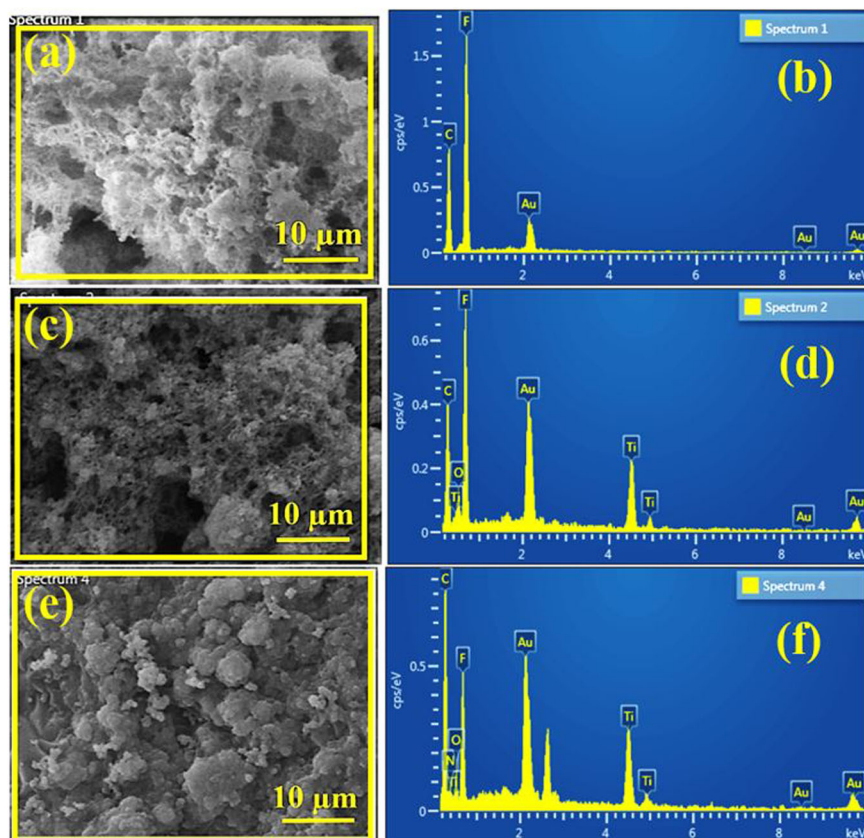
Fig. 7   SEM/EDX analysis of the membranes. EDX analysis of (**a** and **b**) PVDF membrane, (**c** and **d**) TiO$_2$/PVDF membrane, and (**e** and **f**) PPy@TiO$_2$/PVDF membrane.

To confirm the separation of oil from O/W emulsion, the micrographs and photographical images of the feeds and permeates are given in the following Fig. 12. The feeds of different oils including MO, DO, and CO possess many emulsified oil droplets (Fig. 12a, b). Although, the concentration of oil in all different feeds was the same the compositions of oil/water emulsions appeared different under an optical microscope. This variation in the composition of oil/water emulsions reflects the different compositions of oils (MO, Do, and CO) used in the study. The MO oil/water emulsion appeared to have a lesser number of oil droplets (Fig. 12a) while in the case of DO, the emulsion possessed slightly more oil droplets (Fig. 12b). However, in the case of CO oil/water emulsion, the concentration of droplets was the highest (Fig.12c) compared to other oils MO and DO. Since CO contains all the petroleum products including long-chain hydrocarbons and polyaromatic hydrocarbons which generate many bigger-sized oil droplets in the emulsion. This variation in compositions of different oil emulsions is also evident from visual images (Fig. 12d–f). This variation in the composition of different O/W emulsions is responsible for the variation of flux and rejection during O/W emulsion separation filtration experiments (Fig. 11). A visual inspection of photographical images of all feeds and permeates also revealed that permeate-containing vials were clear of any turbidity and cloudiness (Fig. 12d–f). The micrographs of permeate are shown in the following Fig. 12g–i which show that permeates are clear of any oil droplets. The absence of cloudiness and turbidity in permeates confirmed the complete separation of oil from water.

Mechanism of O/W emulsion separation
The O/W emulsion separation can be understood by considering the special surface wettability of the PPy@TiO$_2$/PVDF membrane.

Owing to the presence of superhydrophilic TiO$_2$ NPs and the hydrophilic nature of PPy, the PPy@TiO$_2$/PVDF membrane was rendered as hydrophilic and underwater superoleophobic. The hydrophilic and underwater superoleophobic nature of the PPy@TiO$_2$/PVDF membrane was established based on contact angle (CA) measurements as the underwater oil contact angle ($\theta_{o,w}$) was measured to be >160° which confirmed the underwater superoleophobic nature of the PPy@TiO$_2$/PVDF membrane. Given the hydrophilic nature of the PPy@TiO$_2$/PVDF membrane, the membrane developed a strong hydration layer. The presence of a continuous and strong hydration layer can be attributed to the development of hydrogen bonding. There are numerous hydrogen sites available which can possibly be between the Oxygen atom of TiO$_2$ while another possible site can be a hydrogen bond between water and the N-H group of PPy. The strong hydration layer of water molecules repels the oil droplets from the membrane surface and hence the oil is not able to wet the membrane surface leading to the separation of oil from water. The clean water is permeated through the PPy@TiO$_2$/PVDF membrane while the oil is repelled from the membrane as demonstrated in Fig. 13.

Visible light self-cleaning of PPy@TiO$_2$/PVDF membrane
Although the membrane surface is hydrophilic and underwater superoleophobic, membrane fouling is inevitable due to the highly complex nature of oily feeds. Where most of the oil is rejected, certain components of oily feeds can wet the membrane surface under applied transmembrane pressure. Moreover, the dead-end mode of filtration also aggravates the membrane surface fouling. Hence, the development of fouling cake over the membrane surface with time decreases the performance of the membrane especially the volume of permeate flux is reduced.
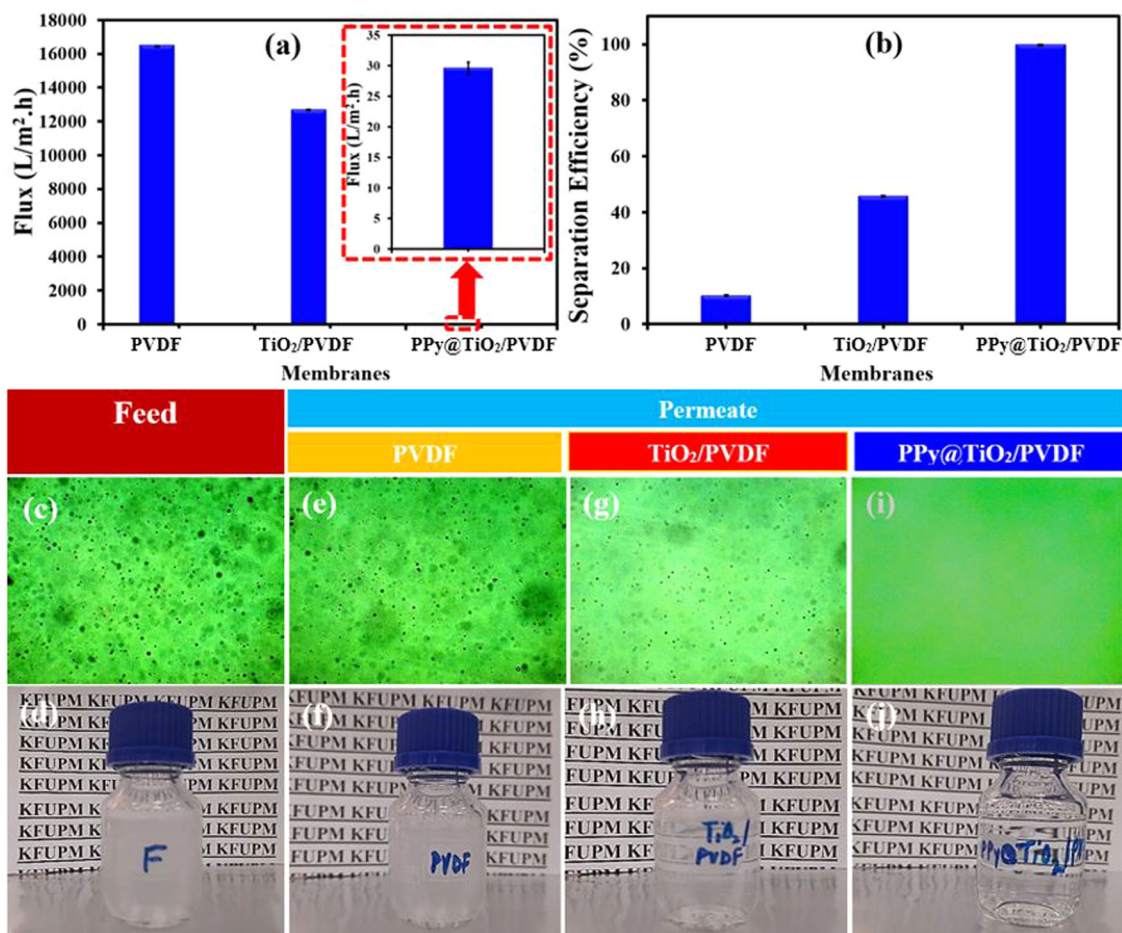
U. Baig and A. Waheed
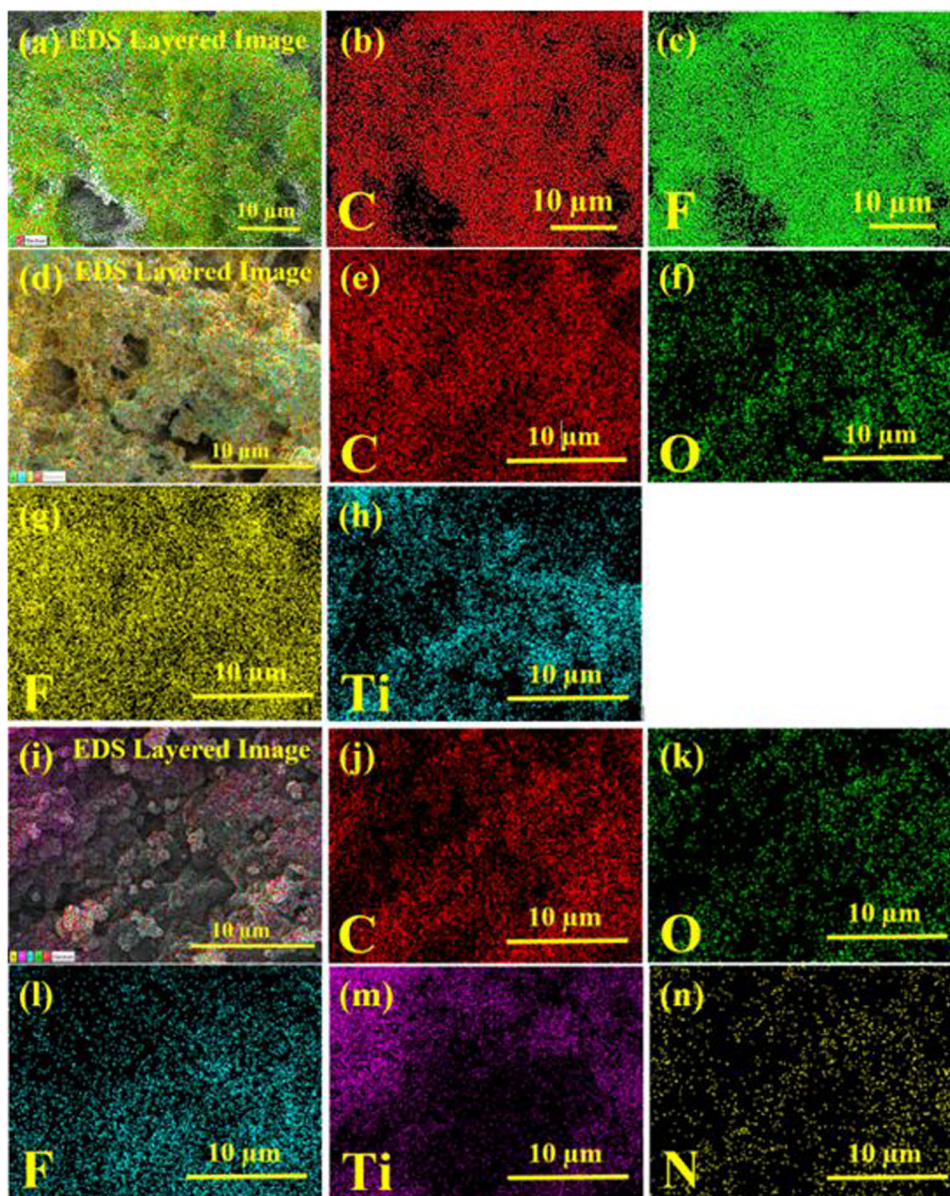
Fig. 8 Elemental mapping analysis of the membranes. Elemental mapping analysis of (**a**–**c**) PVDF membrane, (**d**–**h**) TiO$_2$/PVDF membrane, and (**i**–**n**) PPy@TiO$_2$/PVDF membrane.
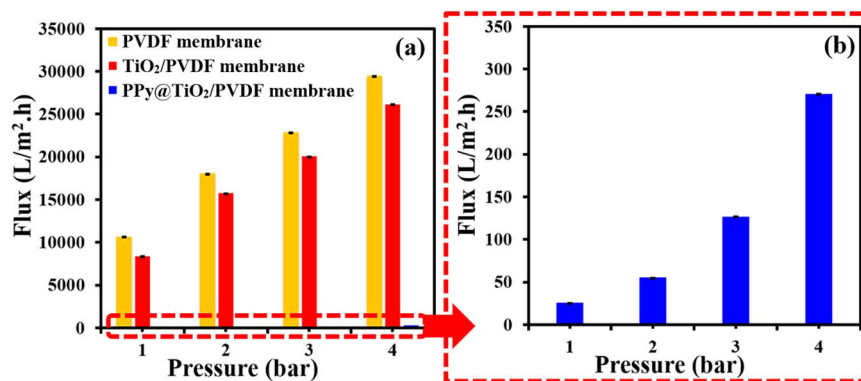
Fig. 9 Variation of pure water flux of PVDF, TiO$_2$/PVDF, and PPy@TiO$_2$/PVDF membranes with varying applied feed pressures. The error bar represents the standard error.
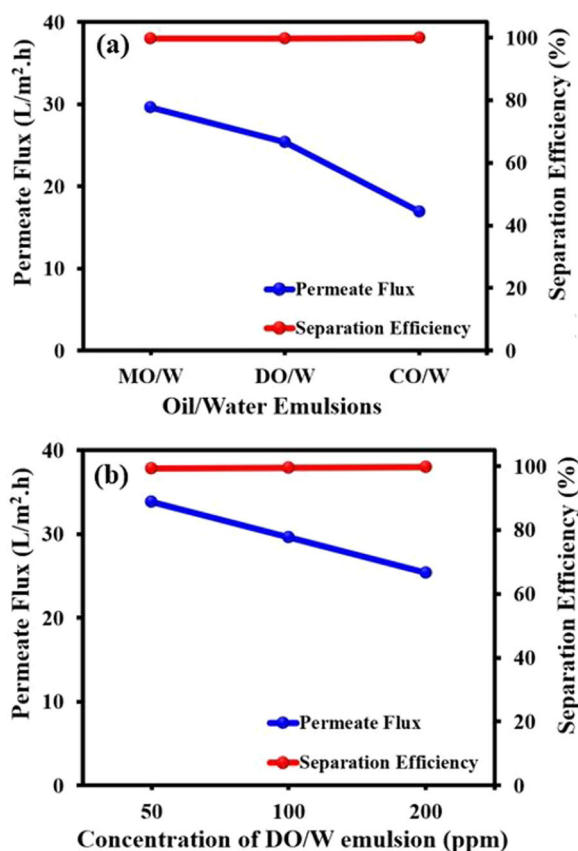
Fig. 10 O/W emulsion separation performance of the membranes, optical & digital images of the feed and permeate samples. Comparison of O/W emulsion separation performance of PVDF, TiO$_2$/PVDF, and PPy@TiO$_2$/PVDF membranes in terms of flux (**a**) and separation efficiency (**b**) at 2 bar using 100 ppm DO/W emulsion. Optical micrographs of feed (**c**) and permeates of PVDF (**e**), TiO$_2$/PVDF (**g**), and PPy@TiO$_2$/PVDF (**i**) membranes. Photographic images of feed (**d**) and permeates of PVDF (**f**), TiO$_2$/PVDF (**h**), and PPy@TiO$_2$/PVDF (**j**) membranes. The error bar represents the standard error.

Therefore, membrane surface cleaning is desperately required to restore the membrane performance over time. Self-cleaning membranes such as PPy@TiO$_2$/PVDF membranes are highly desirable as no external agents are required to clean the membrane surface. As the active layer of PPy@TiO$_2$/PVDF membrane is composed of photocatalytic nanocomposite PPy@-TiO$_2$, the PPy@TiO$_2$/PVDF membrane was readily able to self-clean on exposure to simulated visible solar light. To establish the photocatalytic self-cleaning potential of the PPy@TiO$_2$/PVDF membrane, underwater oil contact angles (OCAs) of fresh, fouled, and cleaned PPy@TiO$_2$/PVDF membrane were measured and compared as shown in Fig. 14. In the case of fouled PPy@TiO$_2$/PVDF membrane, the underwater OCA was decreased from >160° to 80°. Upon exposure of the PPy@TiO$_2$/PVDF membrane to visible light for 1 h, OCA was restored to its original value of >160° (Fig. 14a). The restoration of OCA of PPy@TiO$_2$/PVDF membrane confirmed the self-cleaning potential of the membrane. The self-cleaning of the PPy@TiO$_2$/PVDF membrane was further confirmed by ATR-FTIR of fresh, fouled, and self-cleaned PPy@TiO$_2$/PVDF membrane (Fig. 14b). ATR-FTIR fouled PPy@TiO$_2$/PVDF membrane showed the presence of oil confirmed by two peaks located at 3000 cm^{-1} and 2900 cm^{-1} which are attributed to the deposition of aromatic and aliphatic hydrocarbons of O/W emulsion. However, after self-cleaning the ATR-FTIR of the cleaned membrane resembled the FTIR spectrum of fresh PPy@TiO$_2$/PVDF membrane.

To dig further into the self-cleaning process of the membranes, the performance of the membranes including PVDF, TiO$_2$/PVDF, and PPy@TiO$_2$/PVDF membrane was studied by applying a feed of 100 ppm for a duration of 300 min. The membranes showed a decline in flux due to the deposition of oil on the membrane surface. After 300 min of filtration experiments, the membranes appeared fouled by oil as shown in Supplementary Fig. 1a. Then all the membranes were exposed to a simulated solar light source for 60 min duration for self-cleaning purposes. Compared to PVDF, and TiO$_2$@PVDF membranes, the PPy@TiO$_2$/PVDF membrane showed a comprehensively cleaned surface (Supplementary Fig. 1b). The amount of the oil deposited on the PPy@TiO$_2$/PVDF membrane was found to be 50% of the oil used in the initial feed of 100 ppm which is also reflected in the form of decline in permeate flux. However, after photocatalytic self-cleaning the PPy@TiO$_2$/PVDF membrane showed a considerable recovery in flux. As membrane fouling is inevitable under almost all circumstances, the ways to mitigate self-cleaning can potentially minimize membrane fouling and membranes can be reused significantly. The permeate flux of the TiO$_2$/PVDF membrane was reduced by 96.28% compared to a 65% decline for PPy@TiO$_2$/PVDF membrane. However, after photocatalytic self-cleaning, the PPy@TiO$_2$/PVDF membrane showed a 96.28% recovery in permeate flux whereas TiO$_2$/PVDF membrane showed a recovery of 18% (Supplementary Fig. 2). After studying the recovery in permeate flux, the separation efficiency of the PPy@TiO$_2$/PVDF

Fig. 11 **Effect of different oily feed on O/W emulsion separation performance of the membrane. a** Variation of permeate water flux and separation efficiency with varying types of feeds containing MO, DO, and CO. **b** Variation of permeate water flux and separation efficiency with varying concentrations of DO in water emulsion at 2 bar.

membrane was also studied for 300 min. The PPy@TiO$_2$/PVDF membrane showed a stable performance for the duration of the experiment with a value of O/W separation reaching >99% (Supplementary Fig. 3).

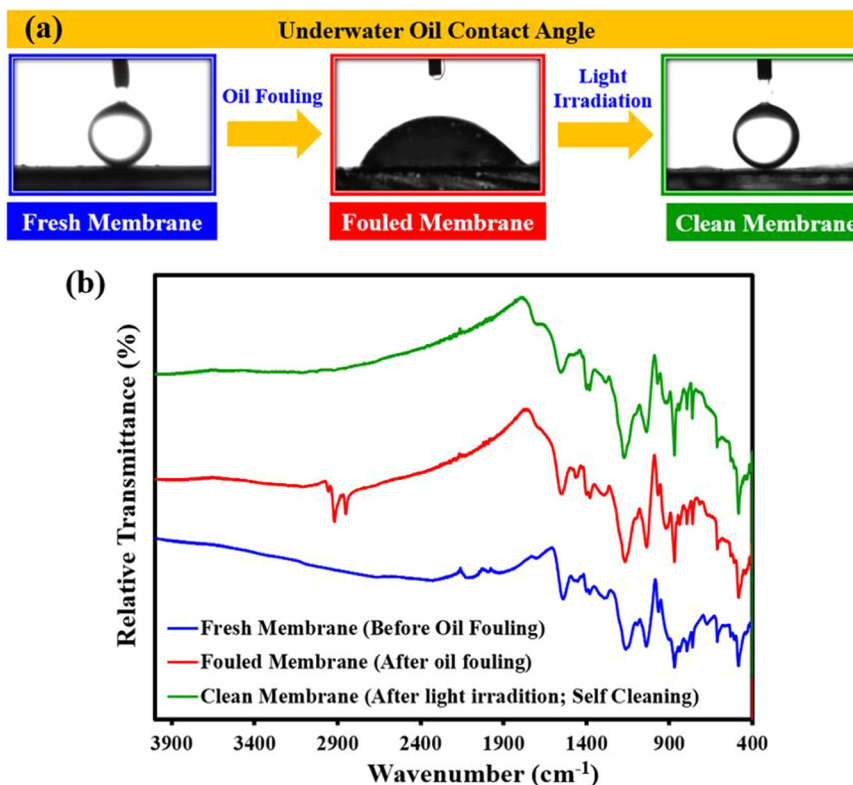## Self-cleaning mechanism of PPy@TiO$_2$/PVDF membrane

The self-cleaning mechanism is demonstrated in the following Fig. 15. As the PPy@TiO$_2$/PVDF membrane is exposed to light sources, the deposited oil is photo-catalytically degraded into CO$_2$ and H$_2$O. It has been established in literature that TiO$_2$ has a band gap of 3.2 eV which can be activated by a wavelength of 388 nm. However, after the introduction of PPy in the case of PPy@TiO$_2$ composite, the band gap was found to be 2.7 eV which can be readily activated by a wavelength of ≈450 nm[17]. The band gaps have been calculated using Tauc plots shown in Supplementary Fig. 4. Because of the lower band gap energy (E$_g$) of the PPy@TiO$_2$, the absorption of a photon of light leads to the excitation of electrons from the highest occupied molecular orbital (HOMO) to the lowest unoccupied molecular orbital (LUMO) and similarly, the electrons are excited from the valance band (VB) of TiO$_2$ to conduction band (CB). However, the CB of TiO$_2$ lies lower in energy than the LUMO of PPy and hence the excited electrons (e$^-$) are transferred from the HOMO of PPy to the CB of TiO$_2$. This transfer of e$^-$ generates holes (h$^+$) in the HOMO of the PPy which are filled by the e$^-$ coming from the VB of TiO$_2$ and hence h$^+$ are created in the VB of TiO$_2$. Hence, a pair of e$^-$ and h$^+$ is created which take part in the photocatalysis. During photocatalysis pairs of e$^-$ - h$^+$ take part in the redox reactions including the reduction of oxygen present on the catalyst surface or reaction medium and oxidation of water leading to the generation of highly reactive oxygen species such as superoxide (O$_2^{.}$) and hydroxide (OH$^-$). Sometimes these species recombine before taking part in the redox reaction resulting in the deceased efficiency of the photo-catalyst. Hence, the separation of this pair is highly essential for photocatalytic activity. During photocatalytic self-cleaning in the case of
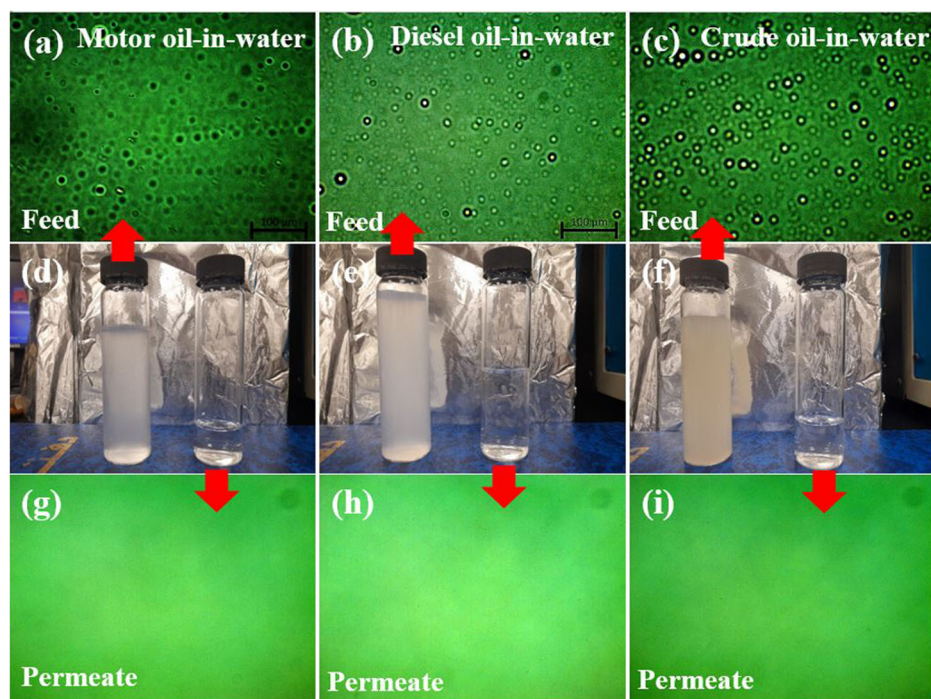
Fig. 12 **Optical and digital images of the feed and permeate samples.** Micrographs of (**a–c**) feeds, (**d–f**) photographical images feeds (turbid sample vials) and permeates (clear sample vials), and (**g–i**) micrographs of permeates collected during oil/water emulsion separation with different oil emulsions at a concentration of 200 ppm at 2 bar.
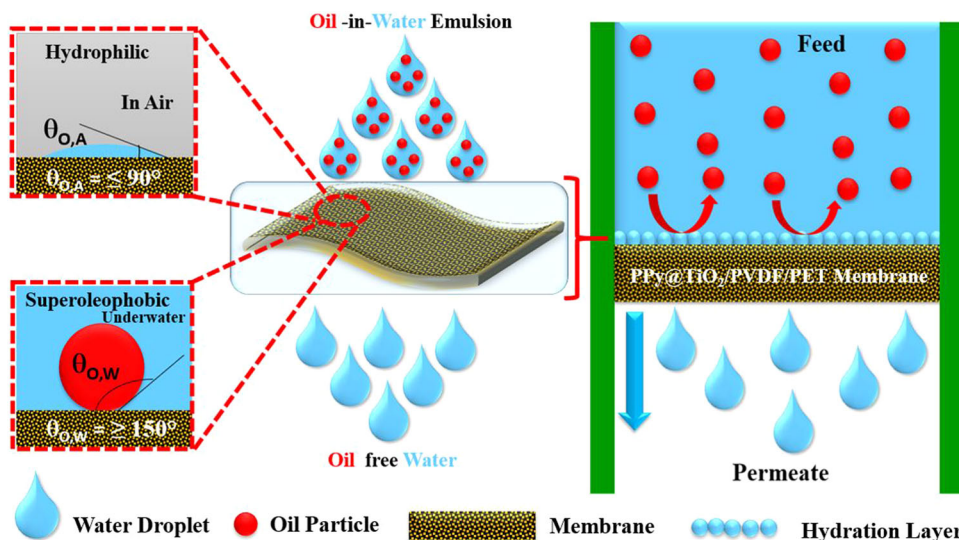
Fig. 13 The proposed mechanism of O/W emulsion separation by PPy@TiO$_2$/PVDF membrane. Image does not contain any third party material.

Fig. 14 Evaluation of self-cleaning performance of the membranes using surface wettability and FTIR spectroscopic analysis. Establishing self-cleaning potential of the PPy@TiO$_2$/PVDF membrane by (**a**) underwater OCAs and (**b**) ATR-FTIR of fresh, fouled, and cleaned membrane. The visible light irradiation time was 1 h.

PPy@TiO$_2$/PVDF membrane, these electrons are absorbed by the oxygen molecules on the surface of the TiO$_2$ in PPy@TiO$_2$/PVDF membrane generating superoxide radicals which in turn degrade the oil adsorbed on the membrane surface. Similarly, the generated holes can also react with water molecules leading to the generation of hydroxyl free radicals. These radicals react with organic pollutants deposited on the PPy@TiO$_2$/PVDF membrane generating CO$_2$ and H$_2$O as biocompatible by-products

(Fig. 15)[11]. A separate experiment was also conducted to establish the photocatalytic potential of PPy@TiO$_2$ composite where PPy@TiO$_2$ composite was also applied for photo-catalytic degradation of methyl orange dye. The methyl orange dye was completely degraded in an hour under simulated light irradiation in comparison to TiO$_2$ which led to 58% photocatalytic dye degradation (Supplementary Fig. 5a). This observation confirmed the photocatalytic potential of PPy@TiO$_2$ composite under visible
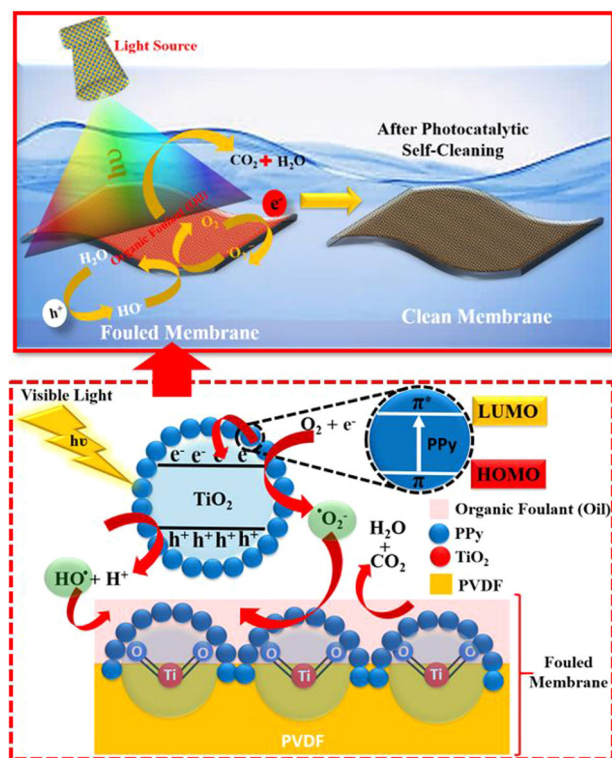
Fig. 15 Proposed photocatalytic self-cleaning mechanism of PPy@TiO$_2$/PVDF membrane under visible light irradiation. Image does not contain any third party material.

light irradiation compared to bare TiO$_2$. Moreover, the PPy@TiO$_2$ composite showed almost double photocatalytic degradation efficiency compared to bare TiO$_2$ (Supplementary Fig. 5b).

The performance of the PPy@TiO$_2$/PVDF membrane has also been compared to other similar membranes where the PPy@TiO$_2$/PVDF membrane has shown a superior performance both in terms of permeate flux and separation efficiency (Supplementary Table 2). This might be attributed to the chemistry of the active layer of the membrane which has also been reflected in WCA by the increased surface hydrophilicity of the PPy@TiO$_2$/PVDF membrane.

In conclusion, a polymeric-inorganic nanocomposite PPy@TiO$_2$/PVDF membrane was fabricated for the sake of reclaiming clean water from oily wastewater feeds along with photocatalytic self-cleaning properties. The TiO$_2$ NPs were dispersed in a coagulation bath and hence upon wet phase inversion the TiO$_2$ NPs were embedded in PVDF matrix. The TiO$_2$@PVDF was used as substrate to grow the PPy polymer through in-situ oxidative polymerization leading to establishment of PPy@TiO$_2$ nanocomposite as an active layer and the resultant membrane was regarded as PPy@TiO$_2$/PVDF membrane. The water contact angle (WCA = $\theta_{w,a}$) in air revealed the hydrophilic nature of the PPy@TiO$_2$/PVDF membrane as WCA reached a value of 52.7° while underwater oil contact angle ($\theta_{o,w}$) which was measured to be >160° confirming the underwater superoleophobic nature of the PPy@TiO$_2$/PVDF membrane. In case of all of the tested feeds containing MO, DO and CO, the rejection was found to be >99%. This higher separation efficiency of PPy@TiO$_2$/PVDF membrane can be attributed to the oxidative polymerization of Py yielding a PPy active layer as confirmed by AFM. A visual inspection of photographical images of all feeds and permeates also revealed that permeate containing vials were clear of any turbidity and cloudiness. In case of fouled PPy@TiO$_2$/PVDF membrane, the underwater OCA was decreased from >160° to 80°. Upon exposure of PPy@TiO$_2$/PVDF membrane to visible light for 1 h, OCA was restored to original value of >160°. Hence, the PPy@TiO$_2$/PVDF membrane has huge potential for cleaning the oily wastewater streams with self-cleaning properties. A recovery of 96.28% in permeate flux was achieved in the case of PPy@TiO$_2$/PVDF membrane.

METHODS

Materials
Polyvinylidene fluoride (PVDF; $[CH_2CF_2]_n$), Polyvinylpyrrolidone (PVP; C_6H_9NO), Dimethylformamide (DMF; C_3H_7NO), Pyrrole (C_4H_4N), Ferric chloride (FeCl$_3$) and Sodium dodecyl sulfate (SDS) were acquired from Sigma (USA). Organic solvents such as Methanol, Iso-propanol, and Ethanol (Fisher Scientific) were purchased from local suppliers.

Fabrication of polymeric/inorganic nanocomposite ultrafiltration membrane
The membrane was fabricated by phase inversion which was followed by in-situ oxidative polymerization. Initially, the PVDF dope solution was prepared by dissolving 15 g of PVDF, 5 g of PVP, and 80 g of DMF. Initially, PVDF was added in DMF, and stirring was continued at 50 °C for 6 h leading to the complete dissolution of PVDF. Upon dissolving PVDF, PVP was added and stirring was continued for 24 h at 50 °C. Then the dope solution was allowed to stand at room temperature to allow all the entraped air bubbles to escape. The dope solution was cast onto a polyester terephthalate (PET) nonwoven fabric prefixed on a glass plate which was immediately immersed in TiO$_2$ nanoparticles containing an isopropanol coagulation bath. The coagulation bath was prepared by dispersing 1 g of TiO$_2$ nanoparticles in 500 mL of isopropanol. The phase inversion was continued for 2 h to allow TiO$_2$ to incorporate in the PVDF membrane while allowing complete demixing of DMF used in dope solution preparation. To enhance the removal of DMF from the PVDF membrane, the isopropanol in the coagulation bath was replaced with DI water, and the membrane was dipped for 24 h leading to TiO$_2$/PVDF/PET Membrane. The next step was the deposition of the polypyrrole (PPy) layer on the TiO$_2$/PVDF/PET Membrane through oxidative polymerization. The pyrrole monomer (2% wt/v) was dissolved in an SDS (100 mg) containing 100 mL DI water solution. The SDS was added to enhance the wettability of the membrane. The TiO$_2$/PVDF/PET Membrane was dipped in a pyrrole-containing solution for 2 h. Upon saturation of TiO$_2$/PVDF/PET Membrane with pyrrole monomer, 100 mL of 2% (w/v) aqueous solution of FeCl$_3$ was added to the solution containing pyrrole saturated TiO$_2$/PVDF/PET Membrane leading to polymerization of pyrrole resulting into the formation PPy active layer on the surface of TiO$_2$/PVDF/PET Membrane. The polymerization of pyrrole was continued for 24 h. The fabricated polymeric/inorganic nanocomposite membrane was regarded as PPy@TiO$_2$/PVDF/PET (PPy@TiO$_2$/PVDF) membrane. Various stages of membrane fabrication are represented in Fig. 1.

Characterization of PPy@TiO$_2$/PVDF membrane
The fabricated PVDF, TiO$_2$@PVDF and PPy@TiO$_2$/PVDF membranes were thoroughly characterized by several membrane characterization techniques. To find the functional groups in the support and the PPy@TiO$_2$/PVDF membrane, ATR-FTIR spectra were recorded. For the sake of recording the spectra, completely dried membrane samples were exposed to laser in ATR mode by using a spectrometer (Nicolet iS50, Thermo). Similarly, surface wettability features of the support and PPy@TiO$_2$/PVDF membrane were determined by contact angle (CA) measuring goniometer (KRUSS, DSA25E). For the sake of measuring CAs, dried pieces of the membranes were cut and fixed on a glass slide using double-sided

tape. Then an appropriate droplet (2 µL) either water or oil was dropped on the membrane surface. The surface roughness of the membranes was measured by atomic force microscopy (AFM) (Agilent 5500 AFM). A piece of the membrane was fixed on a glass support and the surface roughness was measured by taking the average amplitude of cantilever used during measurement. To dig more into the surface features of the support and PPy@TiO$_2$/PVDF membrane, scanning electron microscopy (SEM; JEOL) was carried out. Before, the SEM analysis, the membrane pieces were dried and gold coated for 30 seconds. Energy dispersive X-ray (EDX) and mapping analysis of the supports and PPy@TiO$_2$/PVDF membrane were carried out to find out the elemental composition.

Permeation of experiments of PPy@TiO$_2$/PVDF membrane

Dead-end filtration mode was used to test the O/W emulsion separation potential of the PPy@TiO$_2$/PVDF membrane. Different types of feeds were prepared using motor oil (MO), diesel oil (DO), and crude oil (CO) with varying concentrations of oil 50 ppm, 100 ppm, and 200 ppm. The permeate flux and O/W emulsion separation efficiency were determined to know the performance of the PPy@TiO$_2$/PVDF membrane.

DATA AVAILABILITY

All data generated or analyzed during this study are included in this published article (and its supplementary information files).

REFERENCES

1. Baig, U. & Waheed, A. Exploiting interfacial polymerization to fabricate hyper-cross-linked nanofiltration membrane with a constituent linear aliphatic amine for freshwater production. npj Clean. Water 5, 1–13 (2022).
2. Chen, P. et al. Demulsification and oil recovery from oil-in-water cutting fluid wastewater using electrochemical micromembrane technology. J. Clean. Prod. 244, 118698 (2020).
3. Xie, X. et al. Rapid and efficient oil removal from O/W emulsions by hydrophobic porous polystyrene microspheres embedded with hydrophilic surface micro-regions. J. Hazard. Mater. 434, 128898 (2022).
4. Yan, S. et al. Environmentally safe and porous MS@TiO$_2$@PPy monoliths with superior visible-light photocatalytic properties for rapid oil-water separation and water purification. ACS Sustain. Chem. Eng. 8, 5347–5359 (2020).
5. Daksa Ejeta, D. et al. Preparation of superhydrophobic and superoleophilic cotton-based material for extremely high flux water-in-oil emulsion separation. Chem. Eng. J. 402, 126289 (2020).
6. Jiang, J., Zhang, Q., Zhan, X. & Chen, F. A multifunctional gelatin-based aerogel with superior pollutants adsorption, oil/water separation and photocatalytic properties. Chem. Eng. J. 358, 1539–1551 (2019).
7. Zhao, S. et al. A robust surface with superhydrophobicity and underwater superoleophobicity for on-demand oil/water separation. Nanoscale 13, 15334–15342 (2021).
8. Zhang, S. et al. Cupric phosphate nanosheets-wrapped inorganic membranes with superhydrophilic and outstanding anticrude oil-fouling property for oil/water separation. ACS Nano 12, 795–803 (2018).
9. Verma, V. et al. A review on green synthesis of TiO$_2$ NPs: photocatalysis and antimicrobial applications. Polymers 14, 1444 (2022).
10. Susanto, H. et al. Incorporation of nanoparticles as antifouling agents into PES UF membrane. Mater. Today Proc. 13, 217–223 (2019).
11. Baig, U., Gondal, M. A., Ilyas, A. M. & Sanagi, M. M. Band gap engineered polymeric-inorganic nanocomposite catalysts: Synthesis, isothermal stability, photocatalytic activity and photovoltaic performance. J. Mater. Sci. Technol. 33, 547–557 (2017).
12. Wang, C. F., Huang, H. C. & Chen, L. T. Protonated melamine sponge for effective oil/water separation. Sci. Rep. 5, 1–8 (2015).
13. Chougala, L. S., Yatnatti, M. S., Linganagoudar, R. K., Kamble, R. R. & Kadade-varmath, J. S. A simple approach on synthesis of TiO$_2$ nanoparticles and its application in dye sensitized solar cells. J. Nano Electron. Phys. 9, 04004 (2017).
14. Kaspar, P. et al. Characterization of polyvinylidene fluoride (PVDF) electrospun fibers doped by carbon flakes. Polymers 12, 2766 (2020).
15. Fu, Y. & Manthiram, A. Core-shell structured sulfur-polypyrrole composite cath-odes for lithium-sulfur batteries. RSC Adv. 2, 5927–5929 (2012).
16. Li, L. et al. Underwater superoleophobic porous membrane based on hierarchical TiO$_2$ nanotubes: multifunctional integration of oil–water separation, flow-through photocatalysis and self-cleaning. J. Mater. Chem. A 3, 1279–1286 (2014).
17. Coutts, J. L. Visible-light-responsive photocatalysis: Ag-doped TiO$_2$ catalyst development and reactor design testing. 46th International Conference on Environmental Systems ICES-2016-169, 10-14 July 2016, Vienna, Austria.

ACKNOWLEDGEMENTS

AUTHOR CONTRIBUTIONS

U.B.: Conceptualization, Investigation, Visualization, Data Curation, Methodology, Writing – original draft, Writing – review & editing and A.W.: Conceptualization, Investigation, Visualization, Data Curation, Methodology, Writing – original draft, Writing – review & editing.

COMPETING INTERESTS

The authors declare no competing interests.

ADDITIONAL INFORMATION

Supplementary information The online version contains supplementary material available at https://doi.org/10.1038/s41545-023-00279-1.

Correspondence and requests for materials should be addressed to Umair Baig or Abdul Waheed.

Reprints and permission information is available at http://www.nature.com/reprints

Publisher's note Springer Nature remains neutral with regard to jurisdictional claims in published maps and institutional affiliations.